Progress In Electromagnetics Research B, Vol. 57, 1–20, 2014

Field Measurements within a Large Resonant Cavity Based on the Perturbation Theory

Mohamed Nasserdine, Stephanie Mengué, Christophe Bourcier, and Elodie Richalot*

Abstract—Due to the sensitivity of the field distribution within a resonant cavity to the presence of an object, conventional measurement techniques employing a probe suffer from a limited accuracy. Therefore we propose a new measurement technique of the electric field distribution that avoids the use of a probe. Based on the perturbation theory, it consists of a measure of the cavity resonant frequency variation while displacing a small perturbing object within the cavity. The choice of the perturbing object shape, dimension and material is discussed with the help of simulation and measurement results in a canonical case. The case of reverberation chamber equipped with a mode stirrer is also considered, as well as the insertion of a metallic box within the cavity. Our measurement setup is very low-cost, simple to set up and to use, and adapted to any cavity geometry.

1. INTRODUCTION

Precise field measurements are difficult to attain within a resonant cavity. Indeed, the field distribution within the cavity is very sensitive to the insertion of an object in its enclosure. Thus the measurement antenna or the field probe disturbs the fields; this results in measurement errors.

The present work has been performed in the context of studies on large resonant cavities of moderate quality factor that are reverberation chambers. A reverberation chamber (RC) is a conductive enclosed cavity used for electronic equipment susceptibility or immunity test as well as for antenna characterization [1]. It is used above a minimal frequency [2] from which the statistical field uniformity and isotropy are reached [3]. To insure its adequate performance and calibrate it before performing some tests on a device, some field measurements within the cavity are necessary. More specifically, our measurements performed at low frequencies aimed to better understand the effect of the cavity shape and of the device under test on the field distribution.

The measurement limitations in reverberation chambers were already studied by Arnaut [4] with the spatial averaging effect of the nonzero antenna aperture width and the influence of the antenna itself on the fields. This last influence will be brought to the fore in Section 2 using measurement results. To increase the measurement precision, we propose in this paper a measurement technique based on the perturbation theory [5], which avoids the use of a probe within the working volume of the reverberation chamber. After the presentation of the underlying theory in Section 3, the measurement setup is described in Section 4. It is very low-cost and simple to establish and to use. The sizing of this measurement setup is based on first simulation and measurement results performed in a canonical case in Section 5. While performing measurements first in the analytical case of the empty cavity and then in a cavity equipped with a mode stirrer or a metallic box, we show the ability of this technique to determine the field distribution within a complex cavity. Finally, the method to determine the mode electromagnetic energy is presented and validated in Section 6, and some perspectives are presented to extend the proposed approach to higher frequency measurements.

Received 1 October 2012, Accepted 12 November 2013, Scheduled 21 November 2013

* Corresponding author: Elodie Richalot (elodie.richalot@univ-mlv.fr).

The authors are with the Université Paris Est, ESYCOM (EA 2552), UPEMLV, ESIEE Paris, CNAM, F 77454 Marne-la-Vallée, France.

2. FIELD PERTURBATION DUE TO THE ANTENNA

To simply illustrate the perturbation induced by the measurement system within the resonant cavity, the analytical case of the empty parallelepipedic metallic cavity is considered. We study here the TE061 mode. The electric field is polarized along x-axis, and the variation of E_x amplitude, analytically known, is given by:

$$E_x(x,y,z) \propto \cos\left(\frac{m\pi}{W}x\right)\sin\left(\frac{n\pi}{L}y\right)\sin\left(\frac{p\pi}{H}z\right) \quad (1)$$

with $m = 0$, $n = 6$, $p = 1$.

Measurements are performed within a cavity made of aluminium of dimensions $W = 0.785\,\text{m}$ along x-axis, $L = 0.985\,\text{m}$ along y-axis, and $H = 0.995\,\text{m}$ along z-axis (Fig. 1). For these dimensions, the analytical resonant frequency of the TE061 mode is of 925.44 MHz. Its excitation is performed with a single patch antenna placed at a cavity corner and connected to a RF source situated outside the cavity through a fitted SMA connector.

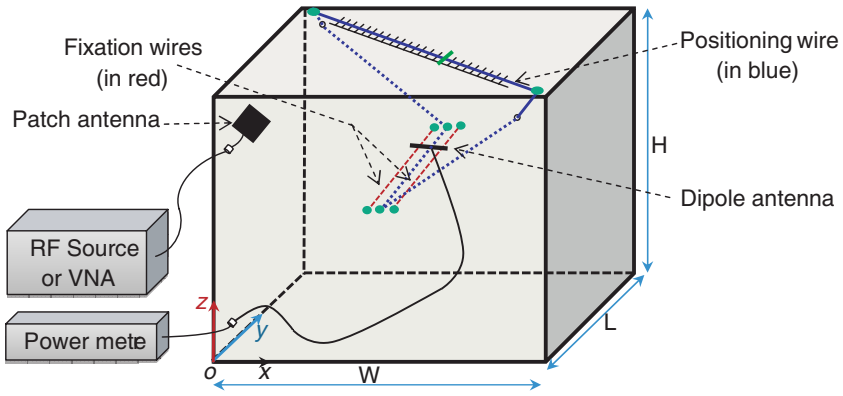

Figure 1. Parallelepipedic cavity loaded by a dipole antenna. Suction pads in green.

A dipole antenna is dedicated to field measurements within the cavity volume. This antenna of length 16 cm is matched at the measurement frequency, i.e., when the antenna is placed in an anechoic chamber, its $|S_{11}|$ parameter is under $-20\,\text{dB}$ from 920 MHz to 930 MHz. It is placed along ($x = W/2$, $z = H/2$) axis, this height corresponding to a maximum of E_x amplitude. Two nylon wires parallel to y-axis ("fixation wires" in Fig. 1), fixed at the cavity walls using four suction pads, permit to maintain the dipole antenna parallel to x-axis. A third nylon wire ("positioning wire") is used for the positioning of the antenna along the fixation wires. This last wire goes out the cavity through small holes initially dedicated to SMA connectors for measurement purpose. A thin cylinder (in green) fixed to the wire and a ruler placed on the cavity permit to control outside the cavity the antenna position within the cavity. The dipole antenna is connected to a power meter situated outside the cavity through a fitted SMA connector.

2.1. Measurements by the Dipole Antenna

For this first measurement, the metallic cavity is excited by the patch antenna connected to a RF source at the frequency 925 MHz. The dipole antenna is connected to a power meter to determine the received power (Fig. 1). A measurement is performed for each position of the dipole antenna along y-axis with a 2 cm-step.

Figure 2 compares the measured electric field amplitude with the theoretical one calculated at the same positions. Both amplitudes are normalized to the unit. To understand the discrepancy between both amplitudes, the influence of the dipole antenna position on the cavity resonant frequency has been examined.

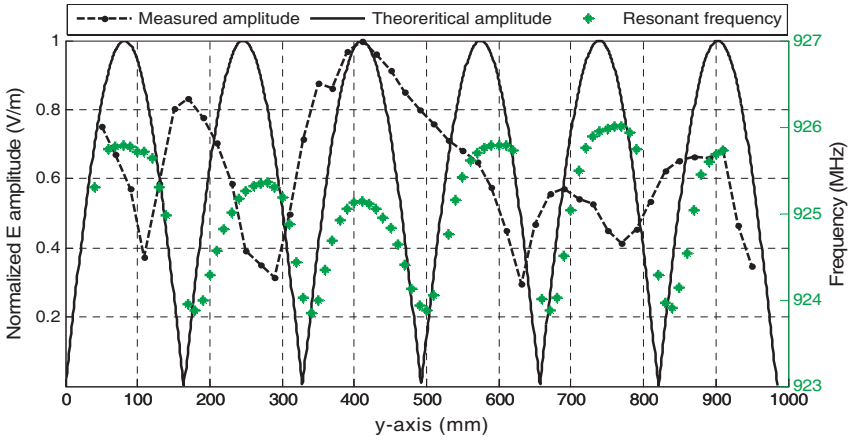

Figure 2. Variation of the normalized measured electric field and the resonant frequency with the dipole antenna position; comparison to the theoretical electric field amplitude.

2.2. Resonant Frequency Variation

The patch antenna is now linked to a Vector Network Analyser (VNA) and the dipole antenna to a matched load connected outside the cavity (so that the antenna cable remains within the cavity). For each position of the dipole antenna along y-axis, the resonant frequency of the cavity is determined from the measurement of the reflection coefficient on a small bandwidth: the resonant frequency is associated to the minimal value of S_{11}.

The amplitude of the reflection coefficient is not given here. However, its minimal value, corresponding to the reflection phenomenon, strongly varies with the dipole antenna position, and for a few positions no resonance can be detected. At these positions, no resonant frequency is thus given.

The variation of the resonant frequency with the dipole antenna position is depicted in Fig. 2. First of all, it can be noticed that the resonant frequency variation is similar to the theoretical amplitude curve. The measured frequency variations are however not symmetrical about the cavity centre due to the presence of the patch excitation antenna and of the dipole antenna cable upsetting the cavity symmetry. This relationship between the resonant frequency variation and the field amplitude, explained in Section 3, will be used in our measurement setup.

The excursion of the resonant frequency is of 2 MHz around 925 MHz. The field magnitude variation around the resonant frequency f_0 follows the expression [5]:

$$\left|\frac{E(f)}{E(f_0)}\right| = \frac{1}{\sqrt{1+\left[2Q\left(\dfrac{f-f_0}{f_0}\right)\right]^2}} \tag{2}$$

In order to determine the Q quality factor of the TE061 resonant mode, the reflection coefficient has been measurement in absence of the dipole antenna; a Q factor of 341 has been deduced from the measured resonance width.

To understand the influence of the resonant frequency variation on the measured field amplitude at 925 MHz, we will consider to extreme cases. We first of all examine the zone around the 5th theoretical electric amplitude peak. The highest measured resonant frequency $f_{\max} = 926.01$ MHz is attained at $y = 770$ mm. For a resonant frequency f_0 of 926.01 MHz and an excitation frequency f of 925 MHz, the ratio of Eq. (2) is of 0.802. This value represents the impact of the resonant frequency perturbation on the measured field amplitude. The measured field amplitude at this position is of 0.411 against a theoretical amplitude of 0.827. Thus the large frequency difference between the resonant frequency and the excitation frequency coincides with a large difference between the theoretical and measured field amplitude.

As a contrary, at $y = 410\,\text{mm}$ corresponding to the third theoretical amplitude peak (unitary theoretical amplitude), the measured resonant frequency is of 925.138 MHz. In this case, the ratio of Eq. (2) is of 0.995. The measured field amplitude at this position also corresponds to the maximal measured field amplitude. Thus, the maximal field amplitude is obtained when a theoretical amplitude peak coincides with a resonant frequency close to the excitation frequency. This is the only area where the match between the resonant frequency and the excitation one is concomitant with a maximum of the mode field amplitude. As a consequence, the measured amplitude in this area is maximal. The measured field amplitude is slightly lower at the other peaks with a resonant frequency far from 925 MHz.

Despite a clear correlation between the measured frequency shift and the discrepancy between the theoretical and measured field amplitudes, the induced frequency shift is not the only cause of field perturbation. Other phenomena are also involved:

- Because of the proximity of the lower and higher resonant modes, the cavity may switch from one mode to another during the antenna translation. Thus 925 MHz corresponds to the resonance of TE061 mode or of the higher order mode depending on the position of the antenna.
- The presence of the dipole antenna induces a local field perturbation.
- Coupling phenomena between the patch and the dipole antennas as well as the influence of the vicinity of cavity walls on the dipole antenna response can also have in impact on the measurement results.
- Due to the length of the dipole antenna, the measurement is non-local and results from a global contribution of the field along the antenna [4]. This phenomenon is however not significant for the TE061 mode due to the invariance of the electric field along y-axis.

Due to the perturbation induced on the field by the measurement system itself, an indirect measurement method will be employed. The field disturbance induced by the measurement setup itself is not specific to resonant cavities, as this problem is also of importance for near-field measurements. In this case, an indirect measurement method, called the modulated scatterer technique (MST) [6, 7], has been developed to limit the field perturbation. For that purpose, the transmission line from the receiving antenna to the measuring instrument is eliminated, the signal picked-up by the probe placed in the near-field of the studied device being reradiated to a distant antenna. Very accurate results are obtained using the MST [8, 9]. However, this technique is not applicable in a resonant cavity. In this case, the probe radiation is not the same as in free space, and the transfer function between two antennas highly varies with their location within the cavity [10]. Therefore, another indirect measurement technique is proposed in this paper to limit the influence of the measurement setup on the field distribution.

3. PERTURBATION TECHNIQUE

In the previous part, the high sensitivity of the cavity resonant frequencies to the position of an object, in this case the dipole antenna, has been put into relief. The perturbation technique takes advantage of this resonant frequency sensitivity to the insertion of an object within the cavity. After the presentation of the underlying theory, we will discuss the choice of the inserted perturbing object before presenting the possible applications of this theory.

3.1. Perturbation Theory

We consider a resonant cavity of volume V composed of vacuum. At the resonant frequency f_0, the electric and magnetic fields within the cavity are E_0 and H_0. It can be noticed that the phase difference between electric and magnetic fields is equal to π. The associated total averaged electromagnetic energy W_0 of the cavity is given by:

$$W_0 = \varepsilon_0 \int\limits_V \left\| \vec{E}_0 \right\|^2 dv = \mu_0 \int\limits_V \left\| \vec{H}_0 \right\|^2 dv \tag{3}$$

The perturbation technique consists of introducing an object within this resonant cavity to observe the perturbation induced on the resonant frequency. According to [5, 11, 12], the insertion of a small

dielectric or metallic object within a resonant cavity results in a frequency shift of the resonant frequency, given by:

$$\frac{f^2 - f_0^2}{f_0^2} = \frac{\mu_0 \int\limits_{V_p} \vec{H}_0 \cdot \vec{M} d\nu - \int\limits_{V_p} \vec{E}_0 \cdot \vec{P} d\nu}{2W_0} \tag{4}$$

where f is the resonant frequency obtained with the perturbation, and V_p is the perturbation volume. P and M are the electric and magnetic polarization densities induced in the inserted object. We can notice that the resonant frequency variation is independent of the total energy within the cavity, so that the presented measurement technique only leads to the relative variation of electric and magnetic fields. We will later see how W_0 can be determined in measurements.

For a small volume V_p of the inserted object, the electric and magnetic fields of the unperturbed cavity, E_0 and H_0, are nearly constant throughout its volume. Eq. (4) can thus be approximated [5]. By neglecting Δf in (f $+\Delta f$) one finds:

$$\frac{\Delta f}{f_0} = \frac{\mu_0 \vec{H}_0 \cdot \vec{M}_m - \vec{E}_0 \cdot \vec{P}_e}{2W_0} \tag{5}$$

where $\Delta f = f - f_0$ and P_e and M_m are the quasi-static electric and magnetic dipole moments induced in the perturbing object by the cavity modal fields (E_0, H_0). These moments depend on the object shape and material, and can be expressed analytically in some canonical cases, as for the homogeneous spheroidal object.

3.2. Spheroidal Sample

In this paper, the chosen perturbing objects are of spherical and cylindrical shapes. Whereas electric and magnetic polarization densities are uniform within a homogeneous spheroid [13], it is not the case for a cylindrical object [14–16]. To avoid this problem and keep an analytical expression of the electric and magnetic dipole moments, the cylinder will be approximate as a spheroid whose two minor axes are equal and very smaller than the major axis [13, 17]. Both perturbing object shapes are thus particular cases of prolate spheroids with $b = c$ and $a \geq b$ (Fig. 3).

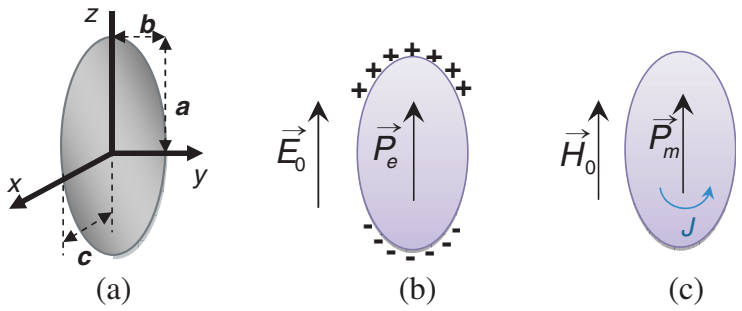

Figure 3. Prolate spheroid sample (a) within a uniform external (b) electric or (c) magnetic field.

Let us consider a prolate spheroid sample, of relative effective (potentially complex) permittivity ε_r^* and relative permeability μ_r, within external electric and magnetic fields as shown in Fig. 3. As already mentioned, due to its small dimensions, the electric and magnetic fields of the unperturbed cavity, E_0 and H_0, are supposed to be constant throughout its volume. These exterior fields induce a polarization charge and a current on the spheroid surface.

The electric and magnetic polarization factors of a prolate spheroid depend on the field source orientation. The dielectric polarization density of a dielectric spheroid sample is [13]:

$$\vec{P} = \varepsilon_0 \bar{\bar{p}}_e \cdot \vec{E}_0 \tag{6}$$

with the electric polarization dyadic:

$$\bar{\bar{p}}_e = \frac{(\varepsilon_r^* - 1)}{1 + (\varepsilon_r^* - 1) l_\perp} \vec{u}_x \vec{u}_x + \frac{(\varepsilon_r^* - 1)}{1 + (\varepsilon_r^* - 1) l_\perp} \vec{u}_y \vec{u}_y + \frac{(\varepsilon_r^* - 1)}{1 + (\varepsilon_r^* - 1) l_{//}} \vec{u}_z \vec{u}_z \tag{7}$$

where $l_{//}$ and $l_\perp$, the electric polarization factors induced by the source field parallel or orthogonal to the major axis, are given by:

$$\begin{cases} l_{//} = \dfrac{1 - e^2}{e^2} \left[\dfrac{1}{2e} \ln \left(\dfrac{e+1}{1-e} \right) - 1 \right] \\ l_\perp = \dfrac{1 - e^2}{2e^2} \left[\dfrac{1}{1 - e^2} - \dfrac{1}{2e} \ln \left(\dfrac{e+1}{1-e} \right) \right] \end{cases} \tag{8}$$

and $e = \sqrt{1 - \left(\frac{c}{a}\right)^2}$ is the eccentricity of the ellipsoid.

Similarly, the magnetic polarization density can be written as:

$$\vec{M} = \bar{\bar{p}}_m \cdot \vec{H}_0 \tag{9}$$

with the magnetic polarizability dyadic:

$$\bar{\bar{p}}_m = \frac{(\mu_r - 1)}{1 + (\mu_r - 1) l_\perp} \vec{u}_x \vec{u}_x + \frac{(\mu_r - 1)}{1 + (\mu_r - 1) l_\perp} \vec{u}_y \vec{u}_y + \frac{(\mu_r - 1)}{1 + (\mu_r - 1) l_{//}} \vec{u}_z \vec{u}_z \tag{10}$$

with magnetic polarization factors equal to the electric ones.

By integrating P and M on the volume V of the spheroid, we obtain the electric and magnetic moments:

$$\vec{P}_e = V \vec{P} \quad \text{and} \quad \vec{M}_m = V \vec{M} \tag{11}$$

where $V = (4/3)\pi\, abc = (4/3)\pi\, ab^2$.

We finally find the relationship between the frequency shift and the sample material properties as well as the electric and magnetic fields at the location of the perturbing spheroid:

$$\begin{aligned} \frac{\Delta f}{f_0} \;=\; & \frac{\mu_0 V}{2W_0} \vec{H}_0 \cdot \left[\frac{(\mu_r - 1)}{1 + (\mu_r - 1)\, l_\perp} H_{0x} \vec{u}_x + \frac{(\mu_r - 1)}{1 + (\mu_r - 1)\, l_\perp} H_{0y} \vec{u}_y + \frac{(\mu_r - 1)}{1 + (\mu_r - 1)\, l_{//}} H_{0z} \vec{u}_z \right] \\ & - \frac{\varepsilon_0 V}{2W_0} \vec{E}_0 \cdot \left[\frac{(\varepsilon_r^* - 1)}{1 + (\varepsilon_r^* - 1)\, l_\perp} E_{0x} \vec{u}_x + \frac{(\varepsilon_r^* - 1)}{1 + (\varepsilon_r^* - 1)\, l_\perp} E_{0y} \vec{u}_y + \frac{(\varepsilon_r^* - 1)}{1 + (\varepsilon_r^* - 1)\, l_{//}} E_{0z} \vec{u}_z \right] \end{aligned} \tag{12}$$

with E_{0i} and H_{0i} the electric and magnetic field components along i-axis.

3.3. Thin Cylindrical Sample

A thin cylinder of radius r and height h along z-axis is approximated as a prolate spheroids with $b = c = r$ and $a = h/2$. In order to quantify the influence of the field components on the frequency shift, we compare the coefficients of the electric polarization dyadic in Eq. (7) using the ratio R defined as follows:

$$R = \frac{p_z}{p_{x,y}} = \frac{1 + (\varepsilon_r^* - 1) l_\perp}{1 + (\varepsilon_r^* - 1) l_{//}} \tag{13}$$

This ratio increases with the relative permittivity amplitude and the ellipsoid eccentricity (Fig. 4). This implies that, for a thin cylinder of high permittivity, the contribution of the electric field components orthogonal to the cylinder axis is negligible in comparison to the one of the component parallel to the cylinder axis. In the presented measurement results (Section 5.1.3), a cylinder of aluminium with $c/a = 0.0174$ is used; at the measurement frequency of 925 MHz, the associated R ratio reaches 440, so that the parallel electric field component can easily be extracted.

Both electric and magnetic fields are influent on the resonant frequency. The term related to the magnetic field increases with the sample permeability, meaning that the magnetic field influence is less important with a paramagnetic metal (as aluminium, $\mu_r \approx 1$) than with a ferromagnetic one (as iron, $\mu_r \gg 1$). For this reason, our measurements will be performed with an aluminium cylinder so that the

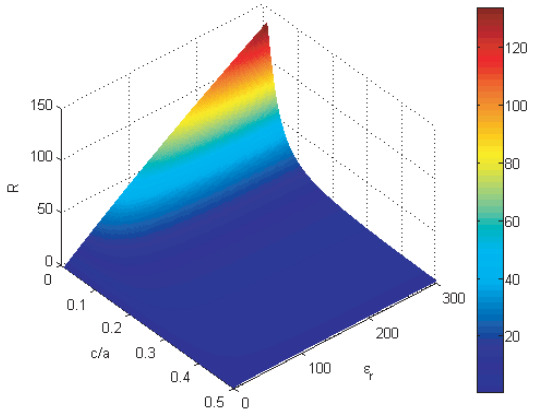

Figure 4. Variation of ratio R versus real permittivity and c/a ratio.

magnetic field remains weakly influent on the resonant frequency. As a consequence, the measure of the resonant frequency perturbation leads to the electric field amplitude along the cylinder axis.

Using Eq. (12), we find the relationship between the frequency shift and the electric field component along z-axis at the location of the cylinder as well as the cylinder permittivity:

$$\frac{\Delta f}{f_0} \approx -\frac{\varepsilon_0 V}{2W_0} \frac{(\varepsilon_r^* - 1)}{1 + (\varepsilon_r^* - 1)\, l_{//}} E_{0z}^2 \tag{14}$$

3.4. Spherical Sample

In the spherical case, the eccentricity vanishes. From the obvious formulae (Eq. (8)), for a dielectric sphere, the electric and magnetic polarization factors are both equal to 1/3 [5].

For a sphere of radius r, placed in initially uniform electric field E_0 and magnetic field H_0, the associated electric and magnetic dipole moments can be calculated as [13, 18]:

$$\vec{P}_e = 4\pi r^3 \varepsilon_0 \frac{\varepsilon_r^* - 1}{\varepsilon_r^* + 2} \vec{E}_0 \tag{15}$$

$$\vec{M}_m = 4\pi r^3 \frac{\mu_r - 1}{\mu_r + 2} \vec{H}_0 \tag{16}$$

Finally, by taking the phase shift between E_0 and H_0 into account, we find:

$$\frac{\delta f}{f_0} = -\frac{4\pi \cdot r^3}{W_0} \left\{ \mu_0 \frac{\mu_r - 1}{\mu_r + 2} \left\| \vec{H}_0 \right\|^2 + \varepsilon_0 \frac{\varepsilon_r^* - 1}{\varepsilon_r^* + 2} \left\| \vec{E}_0 \right\|^2 \right\} \tag{17}$$

In this formula, the effective permittivity and the frequencies are complex. The imaginary part of the resonant frequency, linked to the cavity quality factor [19], is not discussed in this paper.

This relation between the frequency shift and the field amplitudes is a function of the sphere properties i.e., its radius, its permittivity and its permeability. We will examine separately the cases of the metallic and the dielectric inserted object.

In the case of a metallic inserted object, the amplitude of the complex effective permittivity is very large $|\varepsilon_r^*| \gg 1$ and Eq. (17) becomes:

$$\frac{\delta f}{f_0} = -\frac{4\pi \cdot r^3}{W_0} \left\{ \mu_0 \frac{\mu_r - 1}{\mu_r + 2} \left\| \vec{H}_0 \right\|^2 + \varepsilon_0 \left\| \vec{E}_0 \right\|^2 \right\} \tag{18}$$

As for the cylindrical perturbing object, the metallic spheres used in measurements are paramagnetic, as the extraction of the electric field amplitude is easier in this case.

We can also notice that the frequency shift increases with the sphere radius. It implies that the resonant frequency variation will be easier to detect while increasing the sphere size. However, the

hypothesis of a small perturbing object has to be verified, and the increase of the sphere radius results in an integration effect on the fields values. The simulations and measurements presented in Section 5 for different sphere radii have been of help to find a good compromise on the sphere radius.

If a dielectric sphere is chosen, the relative permeability being equal to one, the coefficient before the magnetic field amplitude vanishes and Eq. (17) becomes:

$$\frac{\delta f}{f_0} = -\frac{4\pi \cdot r^3}{W_0}\varepsilon_0 \frac{\varepsilon_r^* - 1}{\varepsilon_r^* + 2} \left\| \vec{E}_0 \right\|^2 \tag{19}$$

In this case the frequency shift is only linked to the electric field and not to the magnetic field, so that the determination of the electric field amplitude is easier. As the modulus of the frequency shift increases with the permittivity amplitude, it remains lower with a dielectric sphere than with a metallic one (for the same sphere radius), and the use of a high permittivity material is recommended for a precise extraction of the field amplitude variation.

In the measurement setup presented in the following, metallic and dielectric spheres have been used. Simulations as well as measurements presented in Section 5 confirm the remarks drawn here.

3.5. Applications of the Perturbation Theory

According to Eq. (12), the shift of the resonant frequency is linked to the inserted sample material properties. The perturbation theory is thus most widely used to characterize the inserted object properties [12, 20]. In this paper, we will take advantage of the sensitivity of the resonant frequency to extract the field properties [21, 22].

The relationship between the resonant frequency variation and the fields within the unperturbed cavity will be used to obtain the electric field distribution through resonant frequency measurements by changing the perturbation location. It has to be mentioned that some measurement setups based on the perturbation theory have already been developed to measure the field distribution within 2D and 3D microwave billiards [23–25] as well as on the central axis of a in superconducting RF cavities for accelerating structures [26]. All the measured cavities presented a very high quality factor which facilitated a precise detection of the resonant frequency; indeed, a high quality factor results in a sharp variation of the measured reflection coefficient and limits the mode overlap.

Our aim in this paper is to adapt this measurement technique to the case of a large resonant cavity of arbitrary shape and of moderated quality factor. To this end, the suited parameters of the measurement setup are investigated and the measurement accuracy is examined.

4. MEASUREMENT SETUP

The measurement setup is similar to the one presented in Section 2, while replacing the dipole antenna by the perturbing object of spherical or cylindrical shape. The fixation wires are only necessary with the cylindrical sample, to maintain it parallel to x-axis. It has to be noticed that the cylinder could also be oriented along y- or z-axes, by an appropriate choice of the sample holes to pass the positioning wire. Fig. 5 shows a sketch of the measurement system with spherical and cylindrical perturbing objects, these objects being in practice used separately.

The cavity resonant frequency is obtained from the reflection coefficient measurement, as it corresponds to its minimum value. The measurement procedure consists of detecting the resonant frequency first for the empty cavity and then with the perturbing object. By moving the inserted object and measuring the resonant frequency associated to each position, we can extract the electric field amplitude variation along the covered path.

Except the VNA and the excitation antenna, our measurement setup only requires very common low-cost objects. Suction pads are used to fix the wires, so that the measurement line position and orientation can easily be changed; measurements can thus be performed everywhere within the cavity. The setup flexibility also concerns the cavity shape, as it could be adapted to every cavity as soon as two small holes permit the positioning wire to come through the cavity walls, but small holes are classically present in order to insert connectors for measurement purposes. Moreover, our measurement setup presents the advantages of being simple to put in and to use, and measurements are rather rapid thanks to an easy displacement of the perturbing object.

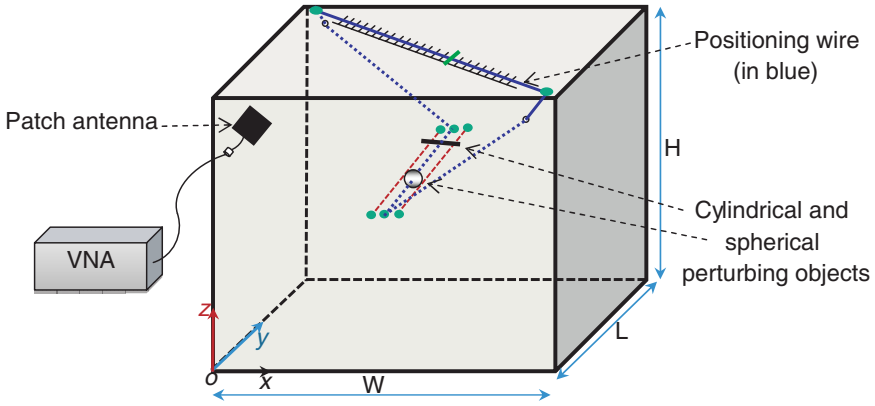

Figure 5. Schematic view of the measurement system with spherical and cylindrical objects inside the cavity.

5. MEASUREMENT RESULTS

To validate our measurement technique and choose the perturbing objects adapted to our resonant cavity, measurements are firstly performed within the empty parallelepipedic cavity, the field expressions being analytically known in this simple case. Measurement results are then presented for the cavity loaded by a mode stirrer and a metallic box.

5.1. Validation with the Empty Cavity

Two resonant modes of the empty parallelepipedic cavity will be considered: the TE021 and the TE061 modes. Before inserting a perturbing object, we first measured the resonant frequencies of the empty cavity excited by the patch antenna. From the position of the minimum reflection coefficient, we deduced measured resonant frequencies of 339.04 MHz for the TE021 mode and 923.78 MHz for the TE061 mode. In comparison to the analytical resonant frequencies (339.60 MHz for the TE021 mode and 925.44 MHz for the TE061 mode), the error is respectively of 0.17% and 0.18%. This shows that the patch excitation antenna only slightly perturbs these frequencies.

Several perturbing objects of different dimensions and materials are alternatively placed along the measurement line ($x_0 = W/2$, $z_0 = H/2$), on which electric and magnetic fields, respectively polarized along x- and z-axes, vary as:

$$E_{0x}(x, y, z) \propto \sin\left(\frac{2\pi}{L}y\right) \quad \text{and} \quad H_{0z}(x, y, z) \propto \cos\left(\frac{2\pi}{L}y\right) \tag{20}$$

The variation of the cavity resonant frequency versus the perturbing object position will be extracted from reflection coefficient measurements performed at each object position.

For validation purposes, the measurement setup, i.e., the cavity loaded by a perturbing object, is simulated using HFSS software, and the cavity resonant frequency is numerically determined for the same object positions as in measurements.

5.1.1. Measurements with a Metallic Sphere

In order to determine the adapted sphere dimension, two metallic spheres of different radii will be used. A sphere of aluminium of radius $r = 25$ mm is firstly used as perturbation in the measurement setup. For each position of the sphere, the reflection coefficient of the cavity is measured using the Vector Network Analyser. Fig. 6 presents one of the measured cavity reflection coefficient around 339 MHz for a fixed position of the sphere. The resonant frequency, corresponding to the minimum of this curve, can easily be determined. In the presented case corresponding to a sphere placed at $y = 6$ cm, it is of 339.010 MHz. The variation of the resonant frequency with the sphere position is presented in Fig. 7.

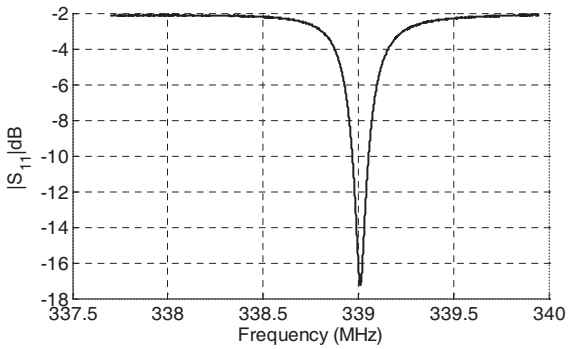

Figure 6. Measured reflection coefficient of the cavity loaded by the metallic sphere ($r = 25\,\text{mm}$).

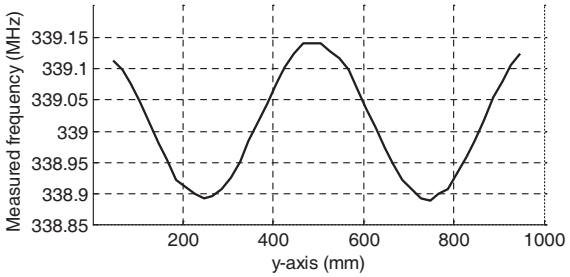

Figure 7. Variation of the resonant frequency with the metallic sphere position ($r = 25\,\text{mm}$).

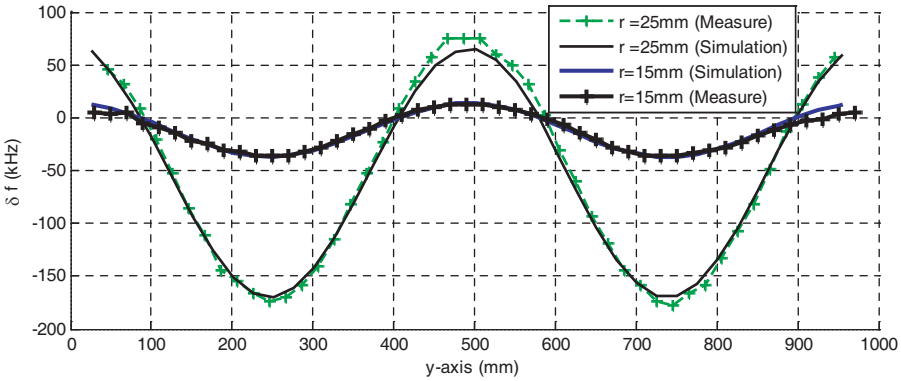

Figure 8. Measured and simulated frequency shift with metallic spheres of radii 25 and 15 mm.

Knowing the resonant frequencies of the empty and loaded cavities, one determines the frequency shift (Fig. 8). The same procedure is followed with an aluminium sphere of radius 15 mm (Fig. 8).

In measurement as well as in simulation, the increase of the frequency excursion with the sphere radius is noticeable. The very small frequency variation obtained with the smallest sphere makes this curve more sensitive to the measurement noise. In our setup, the accuracy of the resonant frequency measurement is limited by the low quality factor of our cavity. Indeed, this parallelepipedic cavity built by our team presents for the studied resonant mode a quality factor around 600 for the TE021 mode. In resonant cavities presenting much higher quality factors, more precise results could be expected with a sphere of small radius.

Similar frequency variations are obtained in simulation and measurement, with a sign change of the frequency shift for both spheres. The measurement line portion on which the frequency shift is positive increases with the sphere radius: the sign change occurs with $r = 15\,\text{mm}$ from $y = 408\,\text{mm}$ to 579, whereas for $r = 25\,\text{mm}$ the frequency shift is positive between $y = 400$ and $587\,\text{mm}$. According to Eq. (18), this positive frequency shift is a consequence of the magnetic field; it can be noticed that the maximal positive frequency shifts are obtained near the walls and at the cavity center, when the electric field is minimum and the magnetic field is maximum. For both perturbing spheres, the maximal amplitudes of the frequency shift correspond to negative values: it shows a preponderant influence of the electric field over the magnetic one.

In order to easily extract the electric field amplitude from the frequency shift variation, the influence of H-field is neglected:

$$\frac{\delta f}{f_0} \approx -\frac{4\pi \cdot r^3}{W_0}\varepsilon_0 \left\|\vec{E}_0\right\|^2 \tag{21}$$

The electric field amplitude is thus given by the normalized square-root of the real frequency shift amplitude. The good concordance between simulations and measurements shows the accuracy of the

measure (Fig. 9). The effect of the sign changes of the frequency shift on the reconstruction of the electric field amplitude is obvious as they result in parasitic arches.

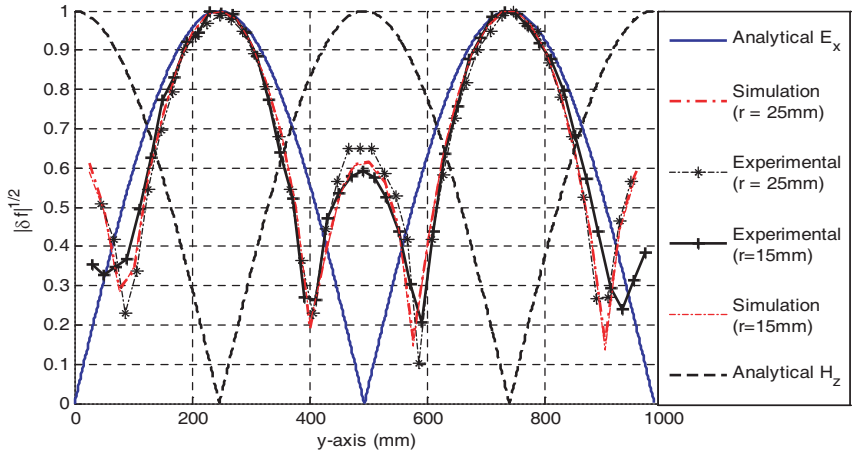

Figure 9. Normalized variations of the square-root of $|\mathrm{Re}(\delta f)|$ and of the analytical amplitude of E_{0x} and H_{0z}. Measurements with metallic spheres of radii 15 mm and 25 mm.

While comparing in Fig. 9 the extracted amplitudes with the analytical variations of E_x and H_{0z} components, one can notice that, when H_{0z} is very small (around $y = L/4$ and $3L/4$), the two experimental and simulated curves follow the variation of E_x value, whereas they follow H_{0z} curve for low E_{0x} values (near the walls and at the cavity centre). Thus the influence of the sphere magnetic polarization disturbs the determination of E_0 amplitude. This indicates that the aluminium spheres are too large to be used as perturbing objects to extract the electric field. However, due to the decrease of the frequency shift amplitude with the sphere radius, the use of a smaller perturbing sphere would require very accurate measurements for a precise extraction of the electric field magnitude variation. Therefore, to eliminate the magnetic field influence, measurements have been performed with a dielectric sphere.

5.1.2. Measurements with a Dielectric Sphere

Two dielectric spheres having the same radii as the metallic ones have been used in measurements. The first one is a sphere of radius $r = 25$ mm made of PVC. The relative permeability of the PVC is equal to one, for a relative permittivity of about 3 in the considered frequency band. As water permittivity is very high (about 80 at room temperature for the studied frequencies), the second perturbing sphere is taken as a plastic sphere covered with wet cotton. Its radius is of 15 mm.

Figure 10 depicts the variation of δf while each sphere moves along the line ($x_0 = W/2$, $z_0 = H/2$). We can notice that, in both cases, the frequency shift remains negative for all the sphere positions. The comparison between the two curves obtained shows that, the frequency shift excursion being lower with the smallest sphere, the frequency measurement is more sensitive to the measurement noise. We also observe that the minimal frequency shift (at the middle of the cavity) is obtained with the smallest sphere.

To extract the electric field variation, we calculate the square-root of these frequency shifts. The normalized curves obtained are in accordance with the variation of E_{0x} analytical amplitude (Fig. 11). The comparison of the experimental results obtained with the dielectric sphere with the ones relative to the metallic sphere having the same radius (Fig. 9) clearly shows the advantage of the dielectric material: the influence of the magnetic field disappears and the electric field amplitude is reconstructed with a satisfying precision.

However, the relatively large radius of the first sphere ($r = 25$ mm) makes the measurement of small field values difficult. The perturbation being non punctual, the frequency shift, related to the field distribution within its volume, represents more precisely the field amplitude when the field spatial

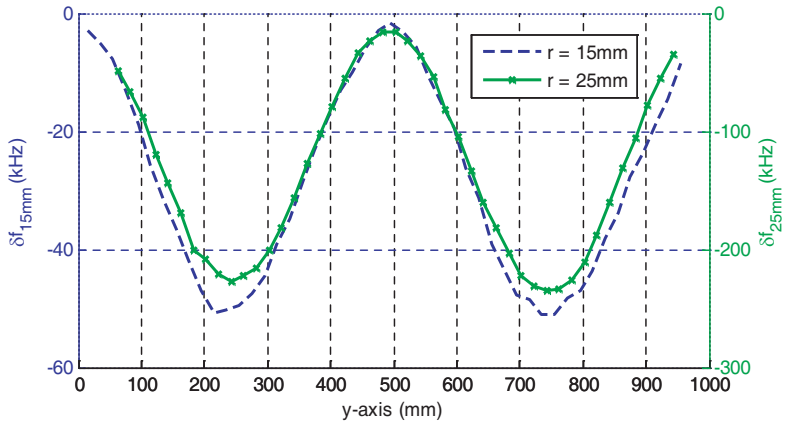

Figure 10. Variations of the δf while moving the dielectric sphere ($r = 15\,\text{mm}$ and $25\,\text{mm}$).

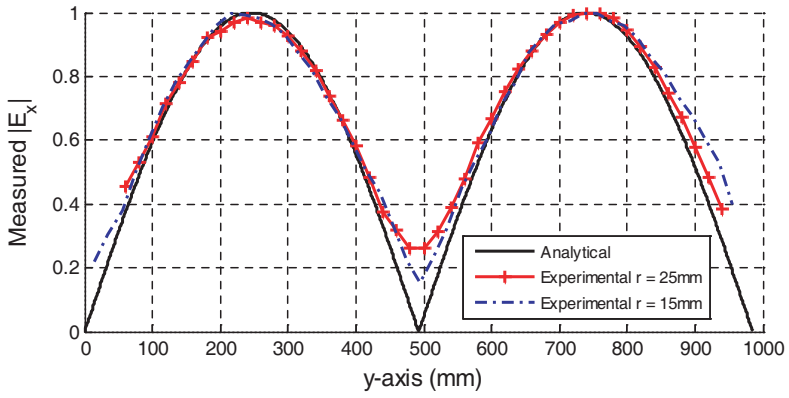

Figure 11. Normalized variations of the square-root of $|\text{Re}(\delta f)|$ and of the analytical amplitude of E_x. Measurements with dielectric spheres ($r = 15\,\text{mm}$ and $25\,\text{mm}$).

variation is slow (as at a maximum of the field amplitude, the derivative being null) as when its spatial variation is rapid (as at a field node).

The advantage of the smallest sphere is a better detection of the electric field node. The use of a dielectric sphere of radius 15 mm is thus adapted to the electric field amplitude measurement of the examined mode. A smaller sphere could permit a better detection of the minimal amplitudes; however to maintain a significant frequency excursion and limit the noise influence, the use of high permittivity dielectric material would be necessary in this case. We remain this limitation is linked to the low quality factor of the studied cavity.

5.1.3. Measurements with a Metallic Cylinder

Measurements are now performed on the TE061 mode along y-axis, as in Section 2. Its measured resonant frequency without any perturbing object is of 923.78 MHz. As the field amplitude spatial variation is faster than with the TE021 mode, the previously used spheres would be too large in regard to the field variation. Therefore, in order to reduce the sample dimension along y-axis while keeping a sufficient frequency shift, a cylindrical sample has been chosen in this case.

A cylinder of aluminium of radius 3 mm and height 11 cm has been placed parallel to x-axis along the measurement line ($x_0 = W/2$, $z_0 = H/2$). As already mentioned in Section 3.3, this cylinder will mainly disturb E_{0x} component, so that we will be able to extract its amplitude.

Figure 12 presents the variation of the frequency shift obtained along the measurement line. It can be noticed that the frequency shift remains negative; this shows the weak influence of the magnetic field

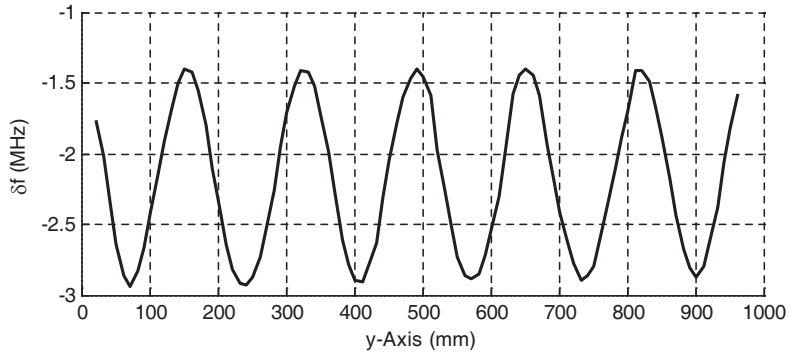

Figure 12. Variations of the δf while moving the metallic cylinder ($r = 3\,\text{mm}$ and $h = 11\,\text{cm}$).

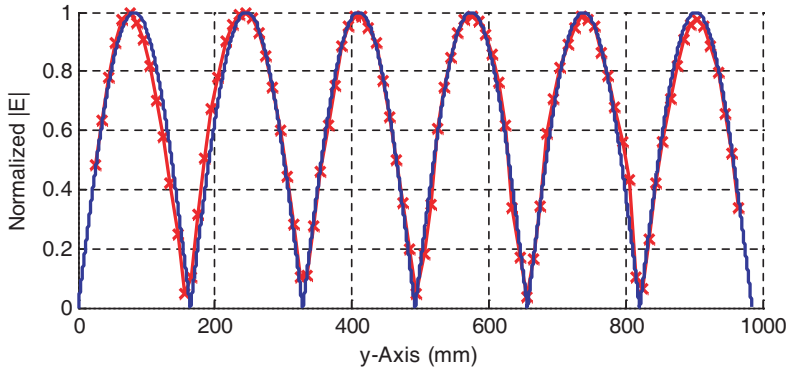

Figure 13. Normalized variations of the square-root of $|\text{Re}(\delta f)|$ (line with crosses) and of the analytical amplitude of E_{0x} (continuous line). Measurements with a metallic cylinder ($r = 3\,\text{mm}$ and $h = 11\,\text{cm}$).

on the resonant frequency perturbation. Moreover, a largers excursion of the frequency shift (about 1.5 MHz) is obtained than with the previous perturbing objects of larger volumes. Fig. 13 compares the normalized extracted E_{0x} amplitude to the analytical one; a good concordance of the two curves is observed.

5.2. Cavity Equipped with a Mode Stirrer

Whereas the previous results are related to a canonical case, the proposed measurement technique is independent of the cavity geometry. To illustrate this versatility, a metallic mode stirrer is now introduced within the previous parallelepipedic cavity (Fig. 14). It consists of a rectangular plate of dimensions 53.8 cm × 19 cm, placed at 10 cm from the cavity bottom and rotated by 30° with regard to y-axis. The excitation patch antenna remains unchanged.

As in this case the solution is no longer analytical, the cavity is simulated using HFSS software, and the electric field amplitude obtained by simulation are compared (Fig. 15) to the ones extracted from measurements along the line ($x_0 = W/2$, $z_0 = H/2$).

Measurements are performed with the spherical dielectric object of radius $r = 15\,\text{mm}$ placed along the observation line. A single excitation patch antenna is considered and the resonant frequency is deduced from the amplitude of S_{11}. The resonant frequency of the empty cavity (with the stirrer but without the perturbing object) is about 924.092 MHz in measurements and 924.309 MHz in simulations.

A good agreement between simulations and measurements is obtained, so that the use of our proposed measurement technique can be considered in a cavity of complex geometry.

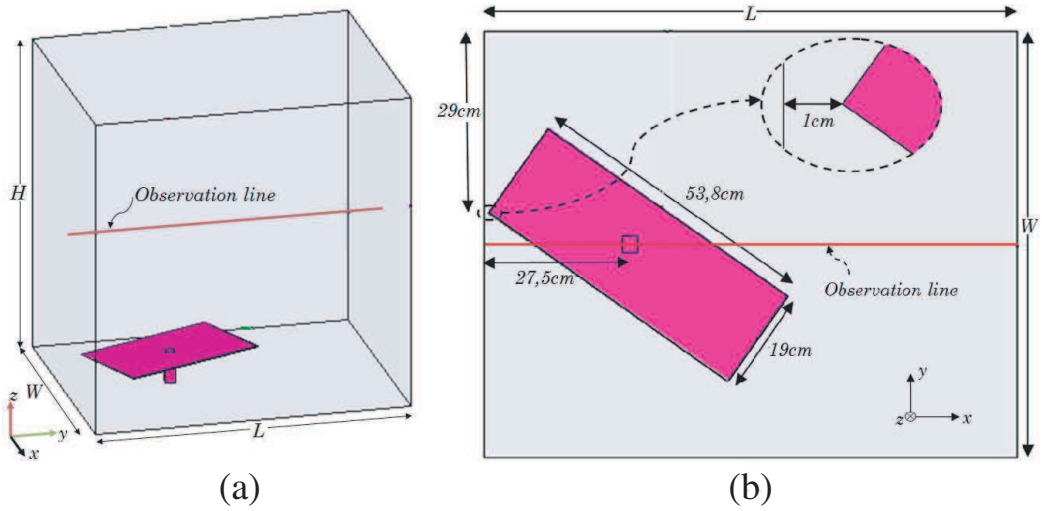

Figure 14. Cavity with a mode-stirrer, (a) 3D view, (b) top view.

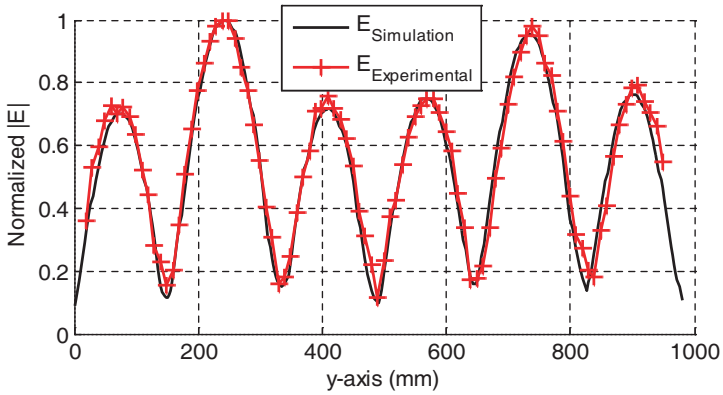

Figure 15. Electric field amplitude variation for the cavity with a mode-stirrer.

5.3. Small Box with Aperture within a Parallelepipedic Cavity

This method is intended to show that the perturbation method could be used for field measurement inside a device under test (DUT). Our measurement approach is particularly useful in this specific case, as the small dimensions of the perturbing object permits measurements through the device apertures.

The system consists of the same parallelepipedic cavity in which a closed aluminium box of dimensions ($L_x = 310\,\text{mm}$, $L_y = 360\,\text{mm}$, $L_z = 560\,\text{mm}$) with two rectangular apertures in inserted (Fig. 16). Both apertures are centred on the measurement line ($x_0 = W/2$, $z_0 = 497.5\,\text{mm}$), and have the same dimensions ($L_s = 100\,\text{mm}$ and $W_s = 50\,\text{mm}$). From now on, the horizontal rectangular aperture is called Slot1, whereas Slot2 refers to the vertical one.

The measurements are performed around 277.2 MHz with a metallic sphere of radius 1 cm and a plastic sphere covered by wet cotton of radius 1.5 cm, the sphere dimensions being here limited by the apertures width. The measured frequency shift variations for both perturbing spheres are presented in Fig. 17. Due to the larger dimension of the dielectric sphere, a wider frequency excursion is observed with this sample.

The radius of the dielectric sphere is bigger than the metallic sample radius, and its diameter, of 3 cm, is close to the aperture width of 5 cm. Therefore, when the dielectric sphere is in proximity of the first aperture Slot1, located around $y = 310\,\text{mm}$, a coupling phenomenon appears and implies at one sphere position a resonant frequency value which is not in concordance with the expected value (peak in Fig. 17). As already mentioned, the perturbation theory relies on the hypothesis of a small

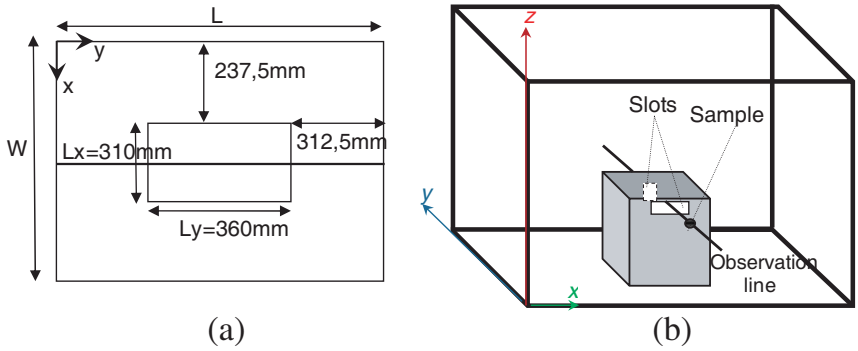

Figure 16. Top (a) and 3D (b) view of the cavity with all elements.

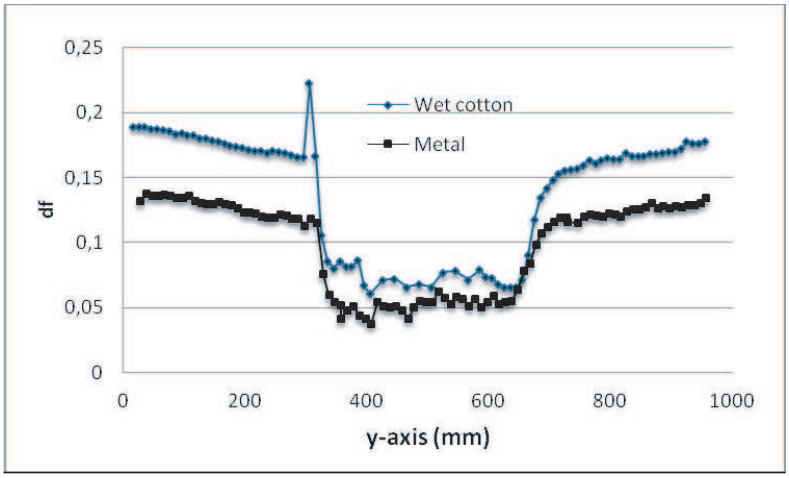

Figure 17. Frequency shift variation with metallic and dielectric spheres.

field perturbation induced by the perturbing object: this hypothesis is not respected at this position. No coupling effect is observed while passing Slot2.

In Fig. 18, measurement results obtained with both perturbing spheres are presented and compared to the simulations results. One can notice that, except for the previously mentioned peak observed at the aperture position, both measurement results are in agreement with simulations.

The used of an E-field probe has been proposed in similar cases [27]. However, it has to be noticed that the E-field probe used in the following (Section 6.1) is too large (53 mm diameter) to pass through these apertures, and that the presence of the optical cable would also disturb this type of measurement. Moreover, a coupling effect appears between the probe and the conducting surfaces so that it is recommended to respect a minimal distance of 100 mm between the probe and conducting planes. The coupling effect observed with the perturbation method is more localized.

6. METHOD ADAPTATION TO THE REVERBERATION CHAMBER

6.1. Determination of the Mode Electromagnetic Energy

Throughout this paper, measurements have been compared to analytical and simulation results obtained without taking the excitation power into account. For the analytical expression, unit amplitude is chosen for the electric field. For the computation of the cavity eigenmodes using the Finite Element Method, a modal approach is adopted [28]. In contrary to the harmonic approach, the excitation antenna and the generator power are not taken into account, and the eigenmodes obtained are of unit electromagnetic energy W_0; a normalization of the electric field is thus necessary while comparing

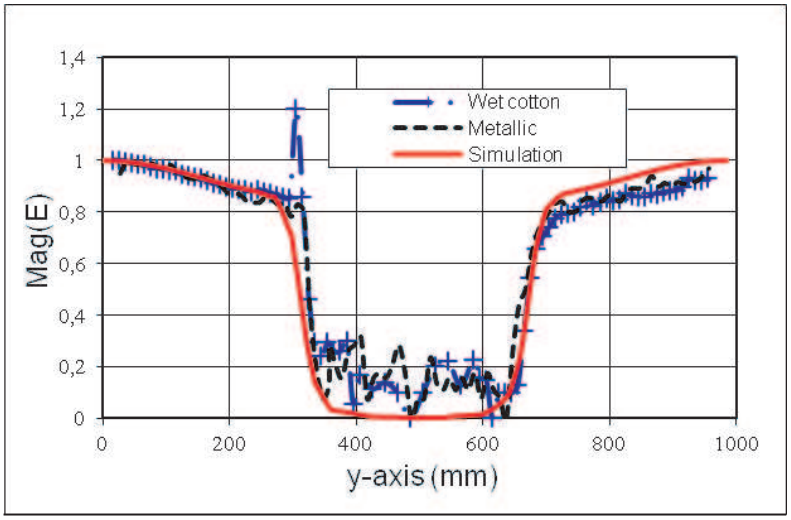

Figure 18. Normalized amplitude of the simulated of extracted electric field.

simulation and measurement results.

However, the experimental determination of the effective field amplitude is possible. The total power received by the antenna loaded by the cavity P_{rec} is simply given by:

$$P_{rec} = \left(1 - |S_{11}|^2\right) \cdot P_{gen} \tag{22}$$

where S_{11} is the system reflection coefficient, and the generator power P_{gen} takes the cables losses into account. The power that is not reflected can be radiated (and contribute to the eigenmode power and the losses within the cavity) or dissipated by the antenna.

The eigenmode power is deduced from the total received power by subtracting the system losses P_{loss}. These last ones, at the resonant frequency f_0, are linked to the system quality factor Q, as [5]:

$$Q = 2\pi f_0 . \frac{W_0}{P_{loss}} \tag{23}$$

This quality factor takes account of losses from various origins [29]: Joule effects in cavity walls, power absorbed in loading objects (as the device under test), leaking of the excitation antenna. For a single mode, the quality factor is experimentally obtained using the formula:

$$Q = \frac{f_0}{f_{BW}} \tag{24}$$

where f_{BW} represents the mode bandwidth.

Thus the measurement of the reflection coefficient of the cavity without the perturbating object leads to the mode electromagnetic energy and consequently to the amplitude of the electric field variation. This allows a complete characterization of the electric field amplitude through measurements using the proposed method.

Let us consider a thin metallic perturbating cylinder parallel to x-axis. According to Eq. (14), one introduces the K factor defined by:

$$|E_x| = K\sqrt{\frac{|\mathrm{Re}(\Delta f)|}{f_0}} \tag{25}$$

where Re(A) design the real part of A, and

$$K = \sqrt{\frac{12W_0 \dfrac{1-e^2}{e^2}\left[\dfrac{1}{2e}\ln\left(\dfrac{e+1}{1-e}\right) - 1\right]}{4\pi r^2 h \varepsilon_0}} \tag{26}$$

The energy W_0 of the empty cavity for a given mode can also be defined as:

$$W_0 = \frac{P_{loss} Q}{2\pi f_0} \tag{27}$$

where P_{loss}, Q and f_0 are respectively the loss power, quality factor and resonant frequency of the mode.

To validate this approach, measurements are performed in the empty cavity for the TE021 mode. Two measurements techniques are employed. The first one is the presented perturbation technique while using a metallic cylinder of radius 1.925 mm and height 11.07 cm oriented along x-axis and moved along the line ($x_0 = W/2$, $z_0 = H/2$). The second measurement technique consists of using an electric field probe PMM EP-600 for a fixed excitation frequency of 339.04 MHz, and to move it along the same line. The results obtained by both methods will be compared.

From S_{21} and S_{11} measured parameters, we deduce the quality factor Q. The electromagnetic averaged energy in the empty cavity is related to the power loss by Eq. (27).

The power of losses is given by:

$$\frac{P_{loss}}{P_{in}} = 1 - |S_{12}(f_0)|^2 - |S_{11}(f_0)|^2 \tag{28}$$

where P_{in} is the excitation power of the antenna. Both values of s-parameters are defined at the resonant frequency of the investigated mode. Then the calculated power loss allows to find the electromagnetic energy of the empty cavity according to Eq. (27). Finally, we find in the measurement case: $Q = 732.34$, $W_0 = 2.57 \cdot 10^{-10}$ J and the K factor is about 500.22 V/m.

The absolute value of the measured electrical field from perturbation theory is shown in Fig. 19. As we can see, the field measured from perturbation exhibits a good fit with the measurements from probe, even for small field amplitudes. The advantages of the perturbation technique over the probe lie in its smaller dimensions and the absence of wires, which permit field measurement within the DUT.

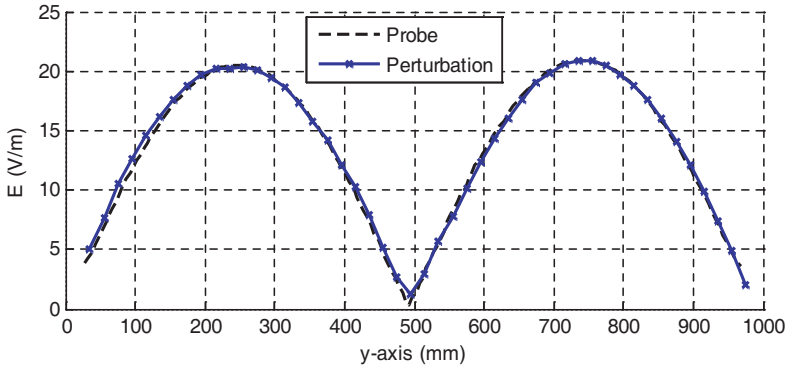

Figure 19. Electrical field measured from the perturbation method and with the probe.

6.2. Regime of Overlapping Resonances

In this paper, the cavity studies are performed at low frequencies, where the resonances can be isolated. At higher frequencies, the modal density increases and mode overlap occurs. In the regime of mode overlap, it becomes difficult to resolve the resonances, whereas the presented perturbation method requires the determination of the resonance frequencies as well as the related quality factor as mentioned in the previous paragraph. Thus this high eigenmode density limits the application of our method in high frequencies.

This overlap phenomenon is increased by the low quality factor of our cavity that widens the resonances. Results could be improved by using a cavity of high quality factor and a small perturbing sample so that the down shifted frequency remains above the frequency of the previous mode.

In [30], Kuhl et al. present an extraction of resonance positions and widths for a microwave cavity in the strong overlapping regime. The Harmonic Inversion method, applied to the measured reflection

coefficient, leads to the complex resonance frequencies (the imaginary part leading to the quality factor) as well as the related reflection coefficient amplitude. In this paper, the extraction of the parameters succeeded for an overlap of up to 12 modes. The precision required by the perturbation method in the determination of the frequency shift could restrict this approach to a lower overlap. However, the extracted complex resonance frequency leading to the only necessary parameters (the resonant frequency and the quality factor) to determine the field properties using the perturbation method, the extension of our proposed technique to the moderate overmoded cavity could be considered.

7. CONCLUSION

As the field distribution within a resonant cavity is very sensitive to the insertion of objects in its enclosure, conventional measurement techniques employed in reverberation chambers suffer from important measurement errors as they necessitate the presence of an antenna or a probe at the measurement location. Therefore, we propose a measurement approach based on the perturbation theory, to avoid the use of this antenna. This indirect approach allows the extraction of the field properties from the variation of the resonant frequency induced by a small inserted object. As shown in this paper, a special attention has to be paid to the choice of the inserted object, as its shape, dimensions and material lead to the measurement of different field properties.

Preliminary simulations and measurements performed in a canonical case have been used to choose perturbing objects appropriated to the studied resonant mode. We firstly considered several spherical perturbing objects, two metallic and two dielectric ones of different radii. Whereas with the metallic sphere the magnetic field can disturb the electric field extraction, the use of a dielectric object leads with good accuracy to the spatial variation of the electric field amplitude. Moreover, the perturbing sphere has to be small enough for a precise reconstruction of the electric field spatial variation, but the resonant frequency variation also needs to be sufficient to be measured with a good accuracy, therefore a compromise has to be found. Finally, the better choice would be to use a small sphere made of a high permittivity dielectric material. Secondly, the extraction of the field amplitude of a single electric field component has been achieved with a good accuracy while using a thin metallic cylinder as a perturbing object.

Good concordance has also been obtained between measurement results and numerical ones, in the more complex cases of a cavity equipped by a mode stirrer or loaded by a metallic box. Therefore, our proposed measurement technique can be proposed as a good candidate for measurements in reverberation chambers. However, some developments remain necessary, in particular to extend this technique to the regime of mode overlap; a track is proposed.

Avoiding the presence of a probe within the cavity that locally disturbs the field distribution, this technique could permit very accurate measurements. Moreover, the measurement setup presents the advantage of being low cost, very simple to install and to use, and easily adaptable to any cavity geometry.

ACKNOWLEDGMENT

The authors wish to express their gratitude to all ESYCOM members who contributed to these measurements. This work was supported by the French National Research Agency (ANR) under the project CAOREV.

REFERENCES

1. Kildal, P.-S., K. Rosengren, J. Byun, and J. Lee, "Definition of effective diversity gain and how to measure it in a reverberation chamber," *Microwave and Optical Technology Letters*, Vol. 34, No. 1, 56–59, Jul. 2002.
2. Hatfield, M. O., M. B. Slocum, E. A. Godfrey, and G. J. Freyer, "Investigations to extend the lower frequency limit of reverberation chamber," *Proc. IEEE Int. Symp. Electromagn. Compat*, Vol. 1, 20–23, Denver, CO, 1998.

3. Hill, D. A., "Plane wave integral representation for fields in reverberation chambers," *IEEE Trans. Electromagn. Compat.*, Vol. 40, No. 3, 209–217, Aug. 1998.
4. Arnaut, L. R., "Effect of local stir and spatial averaging on measurement and testing in mode-tuned and mode-stirred reverberation chambers," *IEEE Trans. Electromagn. Compat.*, Vol. 43, No. 3, 305–325, Aug. 2001.
5. Hill, D. A., *Electromagnetic Fields in Cavity Deterministic and Statistical Theories*, John Wiley&Sons, New Jersey, 2009.
6. Richmond, J. H. and T. E. Tice, "Probes for microwave near-field measurements," *IRE Trans. Microwave Theory and Techniques*, 32–34, Apr. 1955.
7. Justice, R. and V. H. Rumsey, "Measurement of electric field distributions," *IRE Trans. Antennas and Propagation*, 177–180, Oct. 1955.
8. Memarzadeh-Tehran, H., J. J. Laurin, and R. Kashyap, "Optically modulated probe for precision near-field measurements," *IEEE Trans. Instrumentation and Measurement*, Vol. 59, No. 10, 2755–2762, Oct. 2010.
9. Abou-Khousa, M. A., M. T. Ghasr, S. Kharkovsky, D. Pommerenke, and R. Zoughi, "Modulated elliptical slot antenna for electric field mapping and microwave imaging," *IEEE Trans. Antennas and Propagation*, Vol. 59, No. 3, 733–741, Mar. 2011.
10. Rosengren, K., P. S. Kildal, C. Carlson, and J. Carlsson, "Characterization of antennas for mobile and wireless terminals by using reverberation chambers: Improved accuracy by platform stirring," *Microw. Opt. Technol. Lett.*, Vol. 30, No. 20, 391–397, Sep. 2001.
11. Waldron, R. A., "Perturbation theory of resonant cavities," Monograph No. 373 E, The Institution of Electrical Engineers, Apr. 1960.
12. Champlin, K. S. and R. R. Krongard, "The measurement of conductivity and permittivity of semiconductor spheres by an extension of the cavity perturbation method," *IRE Trans. Microwave Theory and Techniques*, 545–551, Nov. 1961.
13. Van Bladel, J., *Electromagnetic Fields*, 2nd Edition, 251, John Wiley&Sons, Inc., New Jersey, 2007.
14. Joseph, R. I., "Ballistic demagnetizing factor in uniformly magnetized cylinders," *Journal of Applied Physics*, Vol. 37, No. 13, 4639–4643, Dec. 1966.
15. Chen, D.-X., J. A. Brug, and R. B. Goldfarb, "Demagnetizing factors for cylinders," *IEEE Tran. Magnetics*, Vol. 27, No. 4, 3601–3619, Jul. 1991.
16. Kobayashi, M. and Y. Ishikawa, "Surface magnetic charge distributions and demagnetizing factors of circular cylinders," *IEEE Trans. Magnetics*, Vol. 28, No. 3, 1810–1814, May 1992.
17. Ao, C. O., K. O'Neill, and J. A. Kong, "Magnetoquasistatic response of conducting and permeable prolate spheroid under axial excitation," *IEEE Trans. Geoscience and Remote Sensing*, Vol. 39, No. 12, 2689–2701, Dec. 2001.
18. Jackson, J. D., *Classical Electrodynamics*, 3rd Edition, John Wiley&Sons, 1999.
19. Slater, J. C., "Microwave Electronics," *Rev. Mod. Phys.*, Vol. 18, No. 4, 441–512, Oct. 1946.
20. Spencer, E. G., R. C. LeGraw, amd F. Reggia, "Measurement of microwave dielectric constants and tensor permeabilities of ferrite spheres," *Proc. of the IRE*, 790–800, Jun. 1956.
21. Maier, L. C. and J. C Slater, "Field strength measurements in resonant cavities," *Journal of Applied Physics*, Vol. 23, No. 1, 68–77, Jan. 1952.
22. Scaglia, C., "Field-strength measurements by perturbation theory," *Electronic Letters*, Vol. 1, No. 7, 200–201, Sep. 1945.
23. Laurent, D., O. Legrand, P. Sebbah, C. Vanneste, and F. Mortessagne, "Localized modes in a finite-size open disordered microwave cavity," *Physical Review Letters*, Vol. 99, 253902, 2007.
24. Kuhl, U., E. Persson, M. Barth, and H.-J. Stöckmann, "Mixing of wavefunctions in rectangular billards," *European Physical Journal B*, Vol. 17, 253–259, 2000.
25. Dörr, U., H. J. Stöckmann, M. Barth, and U. Kuhl, "Scarred and chaotic field distributions in a three-dimensional Sinai-microwave resonator," *Phys. Rev. Lett.*, Vol. 80, No. 5, 1030–1033, Feb. 1998.

26. Som, S., S. Seth, A. Mandal, and S. Ghosh, "Bead-pull measurement using phase-shift technique in multi-cell elliptical cavity," *Proceedings of IPAC2011*, 280–282, San Sebastián, Spain, Sep. 2011.
27. Orjubin, G. and M. F. Wong, "Experimental determination of the higher electric field level inside an overmoded reverberation chamber using the generalized extreme value distribution," *Ann. Telecomm.*, Vol. 66, No. 7–8, 457–464, 2011.
28. Orjubin, G., E. Richalot, S. Mengué, M. F. Wong, and O. Picon, "On the FEM modal approach for a reverberation chamber analysis," *IEEE Trans. Electromagn. Compat.*, Vol. 49, No. 1, 76–85, Feb. 2007.
29. Hill, D. A., M. T. Ma, A. R. Ondrejka, B. F. Riddle, M. L. Crawford, and R. T. Johnk, "Aperture excitation of electrically large, lossy cavities," *IEEE Trans. Electromagn. Compat.*, Vol. 36, No. 3, 169–178, Aug. 1994.
30. Kuhl, U., R. Höhmann, J. Main, and H.-J. Stöckmann, "Resonance widths in open microwave cavities studied by harmonic inversion," *Phys. Rev. Lett.*, Vol. 100, No. 25, 254101, Jun. 2008.